Available online at www.sciencedirect.com
ScienceDirect
Journal of Power Sources 163 (2006) 532–537
JOURNAL OF POWER SOURCES
www.elsevier.com/locate/jpowsour

Short communication

PEM fuel cell open circuit voltage (OCV) in the temperature range of 23 °C to 120 °C

Jianlu Zhang, Yanghua Tang, Chaojie Song, Jiujun Zhang *, Haijiang Wang

Institute for Fuel Cell Innovation, National Research Council of Canada, Vancouver, BC, Canada V6T 1W5

Received 15 June 2006; received in revised form 9 August 2006; accepted 15 September 2006
Available online 27 October 2006

Abstract

Open circuit voltages (OCVs) for a PEM fuel cell operating at 3.0 atm, 100% relative humidity and in the temperature range of 23–120 °C were measured. It was observed that the OCV decreased with increasing temperature. Analysis of the partial O_2 and H_2 pressures in the feed streams revealed that the decrease in partial pressures with temperature were largely responsible for the decrease in OCV. The difference between the theoretical and measured OCVs was analyzed based on the literature, calculations, and hydrogen crossover measurements at OCV. It was concluded that the difference in OCV is caused mainly by two factors, one is the mixed potential of the Pt/PtO catalyst surface, and the other is hydrogen crossover.

Keywords: Open circuit voltage (OCV); High temperature; PEM fuel cells; Apparent exchange current density; Hydrogen crossover; AC impedance

1. Introduction

In recent years, great effort in polymer electrolyte membrane fuel cells (PEMFCs) R&D has been concentrated on increasing the power density, reducing the cost, and improving the reliability/durability [1]. To increase the power density, one approach is to increase the single cell performance. High temperature operation (> 80 °C) of PEMFCs is considered as an effective way to improve the performance in terms of reaction kinetics, catalyst tolerance, heat rejection and water management [2–13]. It follows that high temperature PEM fuel cells are considered to be the next generation of fuel cells.

In the effort to speed-up fuel cell commercialization, the National Research Council of Canada has created a horizontal fuel cell program, from which a high temperature PEM fuel cell project is being funded. In this paper, the open circuit voltages (OCVs) of high temperature PEMFCs in the temperature range of 23–120 °C were found to be temperature dependent, and their values were always lower than the theoretically expected values. To date, a quantitative explanation for such OCV behavior has not been clear in the literature. One explanation attributes this behavior to H_2 crossover and/or internal current, as described in the fuel cell book written by Larminie and Dicks [14]. A mixed potential [15–18] was widely used to interpret the lower open circuit voltage in an acidic medium, when compared to the thermodynamic value of the oxygen electrode (about 1.23 V versus NHE at 25 °C). This mixed potential is a result of the cathodic four-electron oxygen reduction reaction (ORR), and the anodic oxidation that is considered to be either Pt oxidation [18] or the oxidation of impurities [15]. Parthasarathy et al. [12,19,20] employed a micro Pt electrode coated with a thin Nafion membrane, which is similar to a fuel cell cathode/membrane environment, and observed behaviour of the open circuit voltage. The low OCV values, ~0.9–1.0 V (versus NHE), were attributed to the mixed potential and to the effect of contamination. In the effort to obtain a broader picture of this fundamental issue, further investigation using literature data, theoretical calculations, AC impedance spectroscopy and H_2 crossover measurements has been conducted and the results are presented in this paper.

2. Experimental

Nafion 112 and Nafion 117 membranes (DuPont) were used as the proton electrolyte membranes. They were treated in 3% H_2O_2(aq), and then in 1 M H_2SO_4(aq) for 1 h at 60–80 °C, sep-

* Corresponding author. Tel.: +604 221 3087.
E-mail address: jiujun.zhang@nrc.gc.ca (J. Zhang).

0378-7753/$ – see front matter © 2006 Elsevier B.V. All rights reserved.
doi:10.1016/j.jpowsour.2006.09.026

arately, followed by a careful washing step with double distilled water.

Membrane electrode assemblies (MEAs), with an active area of 4.4 cm^2, were prepared by hot pressing the anode, Nafion 112 (or 117) membrane, and cathode together. The anodes and cathodes consist of Pt/Ru (20% PtRu/C, E-TEK) and Pt (40% Pt/C, E-TEK), respectively, with a total Pt loading of 1.0 mg cm^{-2} in each MEA. The MEAs were tested using an in-house single cell hardware fed with 100% RH (relative humidity) H_2 and air at a fixed flow rate of 0.1 L min^{-1}, and 1 L min^{-1}, respectively. A bladder pressure of 100 psig was used to hold the single cell together and provide sufficient electrical contact between the MEA and the graphite bipolar plates.

A Fideris fuel cell test station controlled with FC Power software was used for OCV data collection. Cyclic voltammetry was performed on the fuel cell by simultaneously flushing the cathode compartment with N_2 and the anode with H_2. In this case, the anode served as both the reference and counter electrodes, and the cathode served as working electrode.

Hydrogen crossover was measured using a steady state electrochemical method, during which the fuel cell cathode compartment was flushed with nitrogen to remove O_2, followed by applying a potential of 0.5 V (versus hydrogen reference electrode) relative to the H_2 flushed anode. At this potential, all H_2 that has crossed over from the anode to the cathode should be oxidized (hydrogen oxidation reaction, HOR) giving a current indicative of the amount of hydrogen that has crossed over.

A Solartron FRA 1260 and a Solartron 1287 potentiostat were used for AC impedance measurements at fuel cell open circuit voltage conditions. A perturbing amplitude of 5 mV in the frequency range of 7000–0.1 Hz was employed. The purpose of OCV AC impedance experiments is to obtain the apparent exchange current densities of individual anodic H_2 oxidation and cathodic O_2 reduction reactions.

3. Results and discussion

3.1. Kinetic parameters

According to the Butler–Volmer equation, the cathodic and anodic kinetic current densities can be expressed as Eqs. (1) and (2), respectively [21]:

$$I_c = i^o_{O_2}\left(e^{\frac{n_{\alpha O}\alpha_O F\eta_c}{RT}} - e^{-\frac{n_{\alpha O}(1-\alpha_O)F\eta_c}{RT}}\right)$$

(Cathodic ORR on Pt/PtO) (1)

$$I_a = i^o_{H_2}\left(e^{\frac{n_{\alpha H}\alpha_H F\eta_a}{RT}} - e^{-\frac{n_{\alpha H}(1-\alpha_H)F\eta_a}{RT}}\right)$$

(Anodic HOR on Pt) (2)

In Eqs. (1) and (2), I_c and I_a are the cathodic and anodic current densities, and $i^o_{O_2}$ as well as $i^o_{H_2}$ are the apparent exchange current densities for cathodic O_2 reduction and anodic H_2 oxidation reactions, respectively. For simplicity, it is assumed that $i^o_{O_2}$ and $i^o_{H_2}$ can be used to describe the behaviour of the three-dimensional catalyst layer structure. For an electrode charge transfer controlled process, this assumption should be valid [22,23]. R is the universal gas constant (8.314 J mol^{-1} K^{-1}), and T is the temperature (K). $n_{\alpha O}$ and $n_{\alpha H}$ are the electron transfer numbers in the rate determining steps for cathodic O_2 reduction and anodic H_2 oxidation reactions, respectively. The value of $n_{\alpha H}$ is 1.0, which has been widely reported in the literature [23–25]. For the value of $n_{\alpha O}$, two cases should be considered. The first case is the oxygen reduction polarization curve in the literature has two Tafel slopes [12,19,20,26–28]. In the low current density range (higher cathode potential range where the electrode surface is partially covered by PtO), where the slope is ~60 mV/decade at 25 °C, corresponding to a $n_{\alpha O}$ value of 2.0 for $\alpha_o \approx 0.5$. For the second case, the Tafel slope in the higher current density range is around 120 mV/decade with a $n_{\alpha O}$ value of 1.0, corresponding to a low cathode potential range where the electrode surface is pure Pt. The n_c in Eq. (1) can be expressed as $E^r_c - E_c$, and n_a in Eq. (2) can be expressed as $E_a - E^r_a$, where E^r_c and E^r_a are the thermodynamic electrode potentials (or reversible electrode potentials) for cathodic ORR and anodic HOR, respectively. However, E^r_c can be decreased by a surface Pt–O_2 reaction and H_2 crossover oxidation, which will be discussed in detail in a following section. E_c and E_a are the electrode potentials under operation conditions.

The electron transfer coefficient in Eq. (1), α_o, is a temperature dependent parameter as reported in the literature [12,29–32], and can be expressed as:

$$\alpha_o = \alpha^o_o T \quad (3)$$

where $\alpha^o_{o\text{-Pt/PtO}} = 0.00168\ K^{-1}$ in the temperature range of 25–250 °C. Therefore, Eq. (1) can be rewritten as:

$$I_c = i^o_{O_2}\left(e^{\frac{n_{\alpha O}\alpha^o T F\eta_c}{RT}} - e^{-\frac{n_{\alpha O}(1-\alpha^o T)F\eta_c}{RT}}\right) \quad (4)$$

Eq. (1) or (4) is for cathodic O_2 electroreduction on a Pt/PtO surface. A surface cyclic voltammogram (not shown here) of the cathode showed that when the cathode potential is >~0.8 V (versusNHE) (low fuel cell current density range), the Pt catalyst surface will be covered partially by a PtO layer with surface coverage of ~0.3 [33–35]. Only when the cathode potential is lower than 0.8 V (high current density range), will the catalyst surface be pure Pt. It has been demonstrated that the kinetics of O_2 electroreduction on a pure Pt surface is different from that on a PtO surface [28,36,37]. In this paper, the focus is on the OCV of a PEM fuel cell, therefore, the high current density reaction (where the catalyst surface is pure Pt) will not be perused. For the anode side, the electrode potential is unlikely to become positive enough to result in a PtO surface.

3.2. Apparent exchange current densities for the cathodic ORR

In Eq. (1) or (4) for the cathodic reaction, a critical parameter is the apparent exchange current density ($i^o_{O_2}$), which can be measured using AC impedance spectroscopy at OCV fuel cell conditions.

Fig. 1 shows the fuel cell reaction Nyquist plot at 80 °C, with 3.0 atm of backpressure and at 100%RH. Note that this

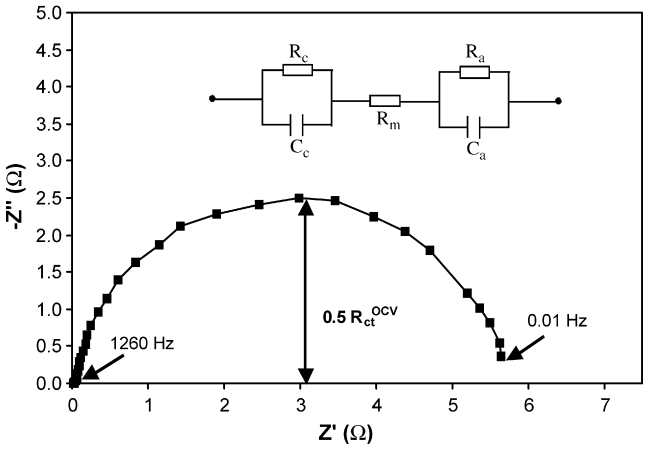

Fig. 1. Nyquist plot for a fuel cell operated at OCV, 80 °C, 3.0 atm, and 100% RH.

Nyquist plot is actually a sum of the impedances contributed by both the anode and the cathode. As a result, the equivalent cathode impedance is much larger than that of the anode by an order of $\sim 10^4$, the measured impedance can be treated as essentially the cathode impedance. At the high frequency end, the *X*-intercept is the membrane resistance (R_m), which is not examined in this paper. The diameter of the semicircle ($R^{OCV}_{ct-O_2}$) is the charge transfer resistance at OCV. A proposed equivalent circuit for the fuel cell reactions is shown as an insert in Fig. 1, where R_c and R_a are the charge transfer resistances for the cathode and anode reactions, respectively. The sum of R_c and R_a is $R^{OCV}_{ct-O_2}$, that is, $R^{OCV}_{ct-O_2} = R_c + R_a$. C_c and C_a are charge transfer related double layer capacitances for the cathode and anode, respectively. Because $R_c \gg R_a$, R_c is equivalent to the $R^{OCV}_{ct-O_2}$ measured. At OCV conditions, if the interrupting voltage is small enough (<5 mV) that the overpotential, η_c, is much smaller than $RT/n_{\alpha O}\alpha_O F$, Eqs. (1) or (4) can then be approximated as:

$$\eta_c = \frac{RT}{n_{\alpha o} F i^o_{O_2}} I_c \tag{5}$$

For AC impedance measurements using a very small AC interrupting voltage at OCV, the obtained $R^{OCV}_{ct-O_2}$ can be expressed as Eq. (6) by differentiating Eq. (5):

$$R^{OCV}_{ct-O_2} = \frac{\partial \eta_c}{\partial I_c} = \frac{RT}{n_{\alpha o} F i^o_{O_2}} \tag{6}$$

Based on Eq. (6), the apparent exchange current density can be calculated if $R^{OCV}_{ct-O_2}$ and $n_{\alpha o}$(=2.0) are known. The obtained apparent exchange current densities for the ORR at different temperatures are listed in Table 1. The data listed in Table 1 will be used for cathode overpotential calculations using H_2 crossover data and Eq. (4).

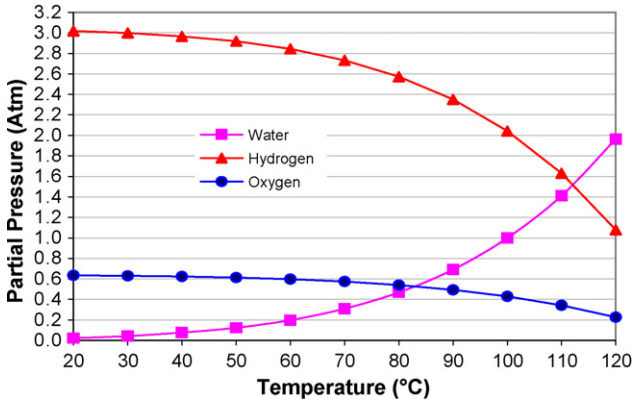

Fig. 2. Partial pressures of O_2, H_2 and H_2O in the fuel cell feed streams as a function of operating temperature, 3.0 atm, and 100% RH.

3.2.1. Fuel cell OCV

A fuel cell open circuit voltage, E^{OCV}, can be expressed as:

$$E^{OCV} = E^r_c - E^r_a \tag{7}$$

where E^r_c and E^r_a can be expressed in the Nernst form shown in Eqs. (8) and (9) separately:

$$E^r_c = E^o_c + \frac{RT}{4F} \ln (P_{O_2} [H^+]^4)$$

$$(\text{For cathode reaction} : O_2 + 4H^+ + 4e^- \rightarrow 2H_2O) \tag{8}$$

$$E^r_a = E^o_a + \frac{RT}{2F} \ln \left(\frac{[H^+]^2}{P_{H_2}} \right)$$

$$(\text{For anode reaction} : H_2 \leftrightarrow 2H^+ + 2e^-) \tag{9}$$

In Eqs. (8) and (9), E^o_c and E^o_a are the standard cathode and anode potentials, respectively. E^o_c is a temperature dependent constant (=1.229 − 0.000846 × (T − 298.15) [38]), E^o_a is zero at any temperature, P_{O_2} and P_{H_2} are the partial pressures (atm) of O_2 and H_2, respectively and $[H^+]$ is the molar concentration of protons (mol L^{-1}). A theoretical OCV can be calculated by deriving Eqs. (8) and (9) to yield Eq. (10):

$$E^{OCV}_{theor} = 1.229 - 0.000846\,(T - 298.15) + \frac{RT}{4F} \ln [P_{O_2} (P_{H_2})^2] \tag{10}$$

Fig. 2 shows the temperature dependent partial pressures of O_2, H_2 and H_2O, respectively, in the feed streams of a fuel cell operating at 100% RH and at 3.0 atm of backpressure. Dramatic drops in partial pressures of O_2 and H_2 are observed when the temperature is higher than ~80 °C. This could be one cause of the decrease in fuel cell performance when the operating temperature is higher than 80 °C, as reported in the author's previous paper [39].

Table 1
Measured apparent exchange current densities at OCV, 3.0 atm, 100% RH and different temperatures

Temperature (°C)	23	40	60	80	100	120
$i^o_{O_2}$ O_2 reduction (A cm^{-2})	1.22×10^{-4}	2.43×10^{-4}	3.92×10^{-4}	4.60×10^{-4}	3.43×10^{-4}	2.24×10^{-4}

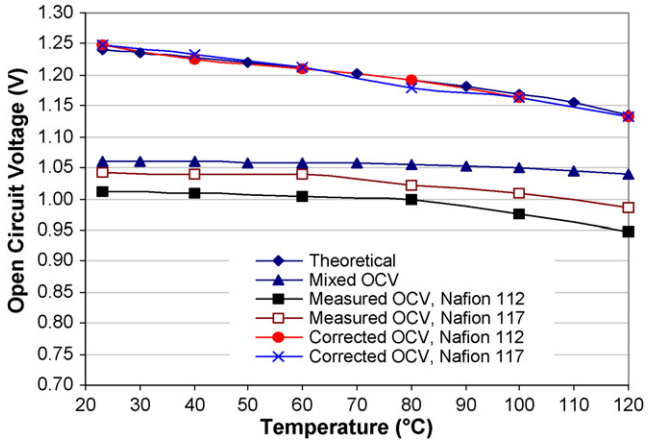

Fig. 3. Fuel cell OCVs as a function of temperature, 3.0 atm backpressure, and 100% RH.

Based on the data shown in Fig. 2, a fuel cell theoretical OCV can be calculated using Eq. (10). Fig. 3 compares calculated temperature dependent OCVs at 3.0 atm backpressure, and 100% relative humidity to those of experimentally tested OCVs. A trend of decreasing OCVs with increasing temperature can be observed. This is mainly caused by the drops in partial pressures of both O_2 and H_2 with increasing temperature.

The measured OCVs ($E^{OCV}_{Measured}$), listed in Table 2, are all lower than the theoretical OCVs (E^{OCV}_{Theor}). The difference between the theoretical and measured OCVs is mainly caused by two different drops in potential ($\Delta E^{OCV}_{Pt-O_2}$ and $\Delta E^{OCV}_{H_2-xover}$ as listed in Table 2). One drop ($\Delta E^{OCV}_{Pt-O_2}$) is caused by a reaction between the Pt surface and O_2, resulting in a mixed cathode potential (E^{OCV}_{mixed}) [12,18–20,35], and the other drop ($\Delta E^{OCV}_{H_2-xover}$) is caused by H_2 crossover from the anode to cathode, reacting with O_2 reducing the O_2 surface concentration, resulting in a decrease in the E^r_c value by an amount equivalent to $\Delta E^{OCV}_{H_2-xover}$.

For a mixed cathode potential, a local-cell mechanism has been put forward to explain the Pt–O_2 reaction mechanism at the electrode in an O_2 saturated acidic solution [18,35,40,41]. The mixed potential is composed of both the cathodic O_2/H_2O reaction potential ($O_2 + 4H^+ + 4e^- \leftrightarrow 2H_2O$, $E^o_c = 1.229V$ (versus NHE)), and the Pt/PtO anode reaction potential ($Pt + H_2O \leftrightarrow PtO + 2H^+ + 2e^-$, $E^o_{Pt/PtO} = 0.88V$ (versus NHE)). The local electrochemical reaction on the Pt surface could create a PtO surface coverage of 30%, and the remaining 70% remains as pure Pt. At steady-state mixed potential, a complete layer of Pt–O can never be achieved in order to keep the reaction of Pt to PtO continued due to the diffusion of Pt–O into the bulk metal. The reported mixed cathode potential is around 1.06 V (versus NHE) at standard conditions (25 °C, 1.0 atm) [18,35] with an O_2 partial pressure dependence of 15 mV atm^{-1}. The temperature dependent values of E^{OCV}_{mixed} listed in Table 2 were calculated based on these mixed cathode potentials. The values of $\Delta E^{OCV}_{O_2-Pt}$ in Table 2 were calculated according to Eq. (11).

$$\Delta E^{OCV}_{O_2-Pt} = E^{OCV}_{Theor} - E^{OCV}_{Mixed} \quad (11)$$

The calculated mixed OCV (E^{OCV}_{mixed}) was also plotted as a function of temperature in Fig. 3 for comparison. Even when the mixed cathode potential is accounted for, ~50–80 mV and ~20–50 mV difference between the mixed OCVs and measured OCVs can still be seen for the MEAs based on Nafion 112 and Nafion 117, respectively. It is believed that this difference is caused by a secondary factor, that is, H_2 crossover. Fig. 4 shows H_2 crossover current densities as a function of temperature for Nafion 112 and Nafion 117 membrane based MEAs. The cathode overpotentials caused by H_2 crossover were calculated based on the H_2 crossover current densities of Nafion 112 and Nafion 117 based MEAs. The corrected curves, which were calculated according to Eq. (12) were also plotted in Fig. 3 for comparison:

$$E^{OCV}_{Corrected} = E^{OCV}_{Measured} + \Delta E^{OCV}_{O_2-Pt} + \Delta E^{OCV}_{H_2-xover} \quad (12)$$

Where the cathode potential decrease caused by H_2 crossover ($\Delta E^{OCV}_{H_2-xover}$) was calculated according to Eq. (4) using the H_2 crossover current density as I_c. In this calculation, it was assumed that H_2 that has crossed over could react with O_2 to produce a corresponding cathodic current density in the same order of magnitude, resulting in a depression of the cathode

Table 2
Open circuit voltages (OCVs) at 3.0 atm, 100% RH and different temperatures

Temperature (°C)	23	40	60	80	100	120
Theoretical open circuit voltage (E^{OCV}_{Theor}) (V)	1.241	1.228	1.210	1.192	1.169	1.136
Measured open circuit voltage ($E^{OCV}_{Measured}$) (V)						
Nafion 117 based MEA	1.011	1.009	1.005	1.000	0.975	0.948
Nafion 112 based MEA	1.042	1.041	1.039	1.021	1.008	0.985
Mixed open circuit voltage (E^{OCV}_{Mixed}) (V)	1.060	1.060	1.059	1.056	1.051	1.040
Open circuit voltage drop caused by surface Pt–O_2 reaction ($\Delta E^{OCV}_{Pt-O_2}$) (V)	0.182	0.168	0.152	0.135	0.119	0.096
Open circuit voltage drop caused by H_2 crossover ($\Delta E^{OCV}_{H_2-xover}$) (V)						
Nafion 117 based MEA	0.025	0.024	0.022	0.024	0.037	0.052
Nafion 112 based MEA	0.054	0.049	0.053	0.056	0.071	0.088
Corrected open circuit voltage ($E^{OCV}_{Corrected}$) (V)						
Nafion 117 based MEA	1.249	1.234	1.213	1.180	1.164	1.133
Nafion 112 based MEA	1.247	1.226	1.210	1.191	1.164	1.133

The fuel cell MEAs were based on Nafion 112 and Nafion 117.

potential. It is believed that the H_2 that has crossed over can form a local half-cell electrochemical reaction on the cathode, such as $H_2 \leftrightarrow 2H^+ + 2e^-$, resulting in a mixed cathode potential in a similar way to that of the half-cell reaction ($Pt + H_2O \leftrightarrow PtO + 2H^+ + 2e^-$) does. When calculating cathode overpotentials at different temperatures using Eq. (4), the apparent exchange current densities of the cathodic reduction reaction listed in Table 1 were used together with a $n_{\alpha O}$ value of 2.0.

As shown in Fig. 3, for both Nafion 112 and Nafion 117 membranes based MEAs, the corrected OCVs are fairly close to the theoretical OCVs, confirming that the difference between the theoretical and measured OCVs is indeed caused by H_2 crossover and the mixed potential. In the literature, the mixed potential on a Pt/PtO surface has been widely used to explain the difference between the theoretical and measured OCVs [12,18–20,35]. H_2 crossover from the anode to cathode that reduces the cathode potential has also been used to interpret this difference [1]. However, on a Pt electrode coated with a thin Nafion membrane, which is similar to a fuel cell cathode/membrane environment, the observed open circuit voltage was also around 0.9–1.0 V (versus NHE) [12,19,20]. Because the measurements were carried out in a half-cell apparatus, no H_2 was present in the electrode assembly. Therefore, this lower OCV in comparison to the mixed potential, was explained as a result of Nafion coating contamination due to impurities rather than H_2 crossover. In order to confirm H_2 crossover caused a reduction in cathode potential at the given fuel cell conditions, a Nafion 117 based MEA, with the same anode and cathode electrodes as the Nafion 112 based MEA, was fabricated and used to obtain fuel cell OCVs at different temperatures. The measured H_2 crossover current densities and OCVs were plotted in Figs. 4 and 5, respectively, together with those of the Nafion 112 based MEA. It is clear that the OCVs of a Nafion 117 based MEA are higher than those of a Nafion 112 based MEA, suggesting that a thicker membrane (Nafion 117, ~175 μm) can give higher OCVs compared to a thinner membrane (Nafion 112, ~50 μm). This is mainly because the H_2 crossover through a thicker Nafion 117 membrane is less than that through a thinner Nafion 112, as shown in Fig. 4. This result confirms that H_2 crossover is indeed one of the two major factors causing a reduction in fuel cell OCVs.

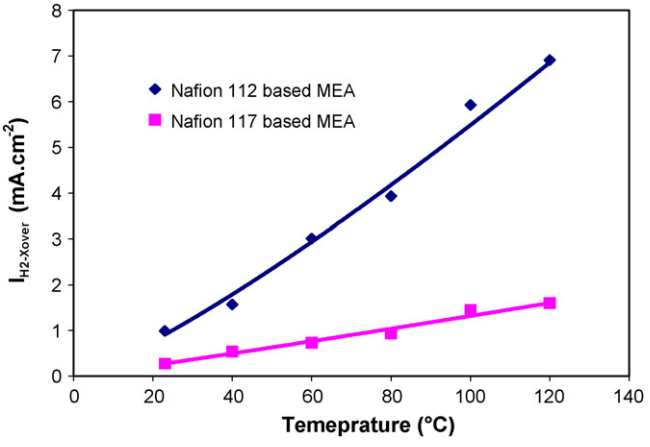

Fig. 4. H_2 crossover current densities as a function of temperature at OCV with different MEAs, 3.0 atm backpressure, 100% RH.

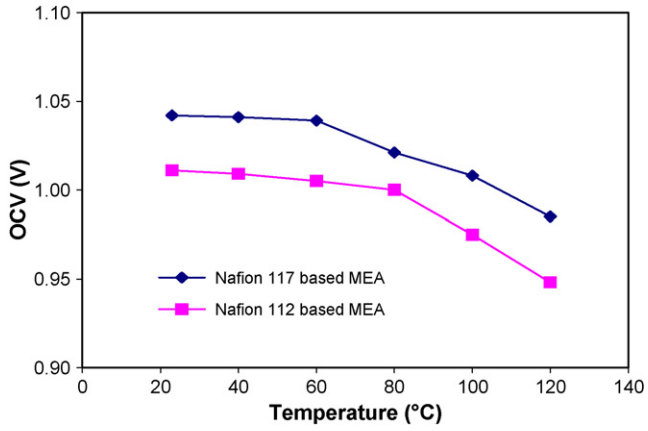

Fig. 5. Measured OCVs as a function of temperature with Nafion 117 and Nafion 112 based MEAs at 3.0 atm backpressure, 100% RH.

4. Conclusion

Temperature dependent OCVs of a fuel cell were obtained in the temperature range of 23–120 °C. The measured OCVs are always lower than the theoretical values. Based on the literature, calculations and experimental measurements, the difference between the theoretical and measured OCVs was mainly caused by two factors. One is the mixed cathode potential and the other is H_2 crossover.

Acknowledgements

The authors would like to thank the financial support from the NRC National PEM Fuel Cell Program and the NRC Institute for Fuel Cell Innovation.

References

[1] J. Larminie, A. Dicks, Fuel Cell Systems Explained, second ed., John Wiley & Sons, Chichester, England, 2000.
[2] P. Costamagna, S. Srinivasan, J. Power Sources 102 (2001) 242.
[3] P. Costamagna, S. Srinivasan, J. Power Sources 102 (2001) 253.
[4] R.K. Ahluwalia, E.D. Doss, R. Kumar, J. Power Sources 117 (2003) 45.
[5] K.T. Adjemian, S.J. Lee, S. Srinivasan, J. Benziger, A.B. Bocarsly, J. Electrochem. Soc. 149 (2002) A256.
[6] Y.-T. Kim, M.-K. Song, K.-H. Kim, S.-B. Park, S.-K. Min, H.-W. Rhee, Electrochim. Acta 50 (2004) 645.
[7] V. Ramani, H.R. Kunz, J.M. Fenton, J. Membr. Sci. 232 (2004) 31.
[8] C. Yang, P. Costamagna, S. Srinivasan, J. Benziger, A.B. Bocarsly, J. Power Sources 103 (2001) 1.
[9] S. Malhotra, R. Datta, J. Electrochem. Soc. 144 (1997) L23.
[10] Z. Qi, C. He, A. Kaufman, J. Power Sources 111 (2002) 239.
[11] H. Xu, Y. Song, H.R. Kunz, J.M. Fenton, J. Electrochem. Soc. 152 (2005) A1828.
[12] A. Parthasarathy, S. Srinivasan, A.J. Appleby, J. Electrochem. Soc. 139 (1992) 2530.
[13] Y. Song, J.M. Fenton, H.R. Kunz, L.J. Bonville, M.V. Williams, J. Electrochem. Soc. 152 (2005) A539.
[14] J. Larminie, A. Dicks, Fuel cell Systems Explained, John Wiley & Sons, Chichester, 2000, 37–59.

[15] H. Wroblowa, M.L.B. Rao, A. Damijanovic, J.O'M. Bockris, J. Electroanal. Chem. 15 (1967) 139.
[16] J.O'M. Bockris, S. Srinivasan, Fuel Cells: Their Electrochemistry, McGraw-Hill Book Company, New York, 1969, Chapter 8, pp.412–468.
[17] A.J. Appleby, J. Electrochem. Soc. 117 (1970) 328.
[18] J.P. Hoare, J. Electrochem. Soc. 109 (1962) 858.
[19] A. Parthasarathy, C.R. Martin, S. Srinivasan, J. Electrochem. Soc. 138 (1991) 916.
[20] A. Parthasarathy, B. Dave, S. Srinivasan, A.J. Appleby, J. Electrochem. Soc. 139 (1992) 1634.
[21] A.J. Bard, L.R. Faulkner, Electrochemical Methods: Fundamentals and Applications, second ed., John Wiley, New York, 2001, 87–136.
[22] J. Zhang, H. Wang, D.P. Wilkinson, D. Song, J. Shen, Z. Liu, J. Power Sources 147 (2005) 58–71.
[23] W. Vogel, J. Lundquist, P. Ross, P. Stonehart, Electrochim. Acta 20 (1975) 79.
[24] Junhua Jiang, Anthony Kucernak, J. Electroanal. Chem. 567 (2004) 123.
[25] N.M. Markovic, B.N. Grgur, P.N. Ross, J. Phys. Chem. B 101 (1997) 5405.
[26] A.J. Appleby, B.S. Baker, J. Electrochem. Soc. 125 (1978) 404.
[27] A. Damjanovic, M.A. Genshaw, Electrochim. Acta 15 (1970) 1281.
[28] A. Damjanovic, V. Brusic, Electrochim. Acta 12 (1967) 615.
[29] A.J. Appleby, J. Electroanal. Chem. 24 (1970) 97.
[30] E. Yeager, Electrochim. Acta 29 (1984) 1527.
[31] S.J. Clouser, J.C. Huang, E. Yeager, J. Appl. Electrochem. 23 (1993) 597.
[32] A. Damjanovic, J. Electroanal. Chem. 355 (1993) 57.
[33] K. Nagerl, H. Dietz, Electrochim. Acta 4 (1961) 1.
[34] H. Dietz, H. Gohr, Electrochim. Acta 8 (1963) 343.
[35] R. Thacker, J.P. Hoare, J. Electroanal. Chem. 30 (1971) 1.
[36] A. Damjanovic, J.O'M. Bockris, Electrochim. Acta 11 (1966) 376.
[37] D.T. Sawyer, R.J. Day, Electrochim. Acta 8 (1963) 589.
[38] J.C. Amphett, R.M. Baumert, R.F. Peppley, P.R. Roberge, T.J. Harris, J. Electrochem. Soc. 142 (1995) 9.
[39] Y. Tang, J. Zhang, C. Song, H. Liu, J. Zhang, H. Wang, S. Mackinnon, T. Peckham, J. Li, S. McDermid, P. Kozak, J. Electrochem. Soc. 153 (2006) A2036.
[40] A.J. Bard, H. Lund, Encyclopaedia of Electrochemistry of the Elements, M. Dekker, New York, 1973, Chapter Ixa-3.
[41] C. Wagner, W. Traud, Z. Elektrochem. 44 (1938) 391.